IEEE Access
Multidisciplinary | Rapid Review | Open Access Journal

Received May 16, 2019, accepted June 13, 2019, date of publication June 19, 2019, date of current version July 9, 2019.

Digital Object Identifier 10.1109/ACCESS.2019.2923666

Dual-Band MIMO Antenna With Compact Self-Decoupled Antenna Pairs for 5G Mobile Applications

ZHOUYOU REN, (Member, IEEE), AND ANPING ZHAO, (Senior Member, IEEE)
Shenzhen Sunway Communication Company Ltd., Shenzhen 518057, China

Corresponding author: Anping Zhao (anping.zhao@sz-sunway.com)

This work was supported in part by the Shenzhen Science and Technology Innovation Committee under Project 20170237 and Project 20180156, and in part by the Shenzhen Development and Reform Commission under Project 20171393.

ABSTRACT In this paper, a dual-band four-element multi-input and multi-output (MIMO) antenna system based on compact self-decoupled antenna pairs is proposed for the fifth-generation (5G) operation in mobile terminals. By sharing one common grounding branch for the two adjacent antenna units, dual-band antenna pairs with high isolation can be obtained. In particular, the two compact antenna pairs are placed perpendicularly on both sides of the system ground plane. The MIMO antenna system is optimized to operate in both 3.5 GHz (3.4–3.6 GHz) and 4.9 GHz (4.8–5.0 GHz) bands with isolation better than −17.5 dB for the low band and −20 dB for the high band. The proposed dual-band four-antenna MIMO system is fabricated and measured, and a good agreement between the simulation and measurement is obtained. Moreover, the influences of the phantom hand and display panel on the performance of the MIMO antenna system are also studied and discussed.

INDEX TERMS 5G, MIMO system, mobile antennas, self-decoupled antenna pairs, sub-6GHz.

I. INTRODUCTION

The fifth generation (5G) mobile communication system will be deployed on a large-scale in 2020, and it will bring us many advantages such as higher transmission rate and shorter latency over the current 4G system [1], [2]. It has been demonstrated in [3]–[23] that to improve the data throughput in a multipath environment for 5G operations, the multiple-input and multiple-output (MIMO) antenna system should be adopted. Due to the compact volume of mobile terminals, however, how to achieve better antenna performance for the MIMO antenna system in terms of high antenna isolation and low envelope correlation coefficient (ECC) becomes a challenge. In the past, numerous studies have focused on improving the isolation of the MIMO antenna systems by using the neutralization line [4]–[6], the polarized antenna [7]–[9], the asymmetrically mirrored antennas [10]–[12], the multimode decoupling technique [13], the self-isolated antenna element method [14], [15], as well as the orthogonal-mode pair [16]. Among the above designs [3]–[22], however, the dual-band operations were considered only in [5], [6], [11], [21], and [22], which will more or less restrict the application in the 5G terminals. This is because different countries or operators may use different bands, thus dual-band operations are usually needed for the roaming purpose [24].

In this paper, a dual-band 4-antenna MIMO system based on the self-decoupled antenna pair is proposed. In particular, by placing two adjacent antenna elements of the antenna pair very close to each other and by arranging the two antenna elements to share one common coupled grounding branch, very good antenna isolation can be obtained. The proposed MIMO antenna can cover both 3.5GHz band (3.4-3.6GHz) and 4.9GHz band (4.8-5.0GHz), which are authorized by the Ministry of Industry and Information Technology of China for the 5G application [25]. Due to the self-decoupled structure, isolations better than −17.5dB for the 3.5GHz (low band) and −20dB for the 4.9GHz (high band) can be obtained. In addition, the performance of the proposed self-decoupled MIMO antenna system is verified by both simulation and measurement.

II. THE COMPACT DUAL-BAND MIMO ANTENNA SYSTEM

A. ANTENNA CONFIGURATION OF THE 4-ANTENNA MIMO SYSTEM

Fig. 1 shows the detailed geometry of the proposed dual-band 4-antenna MIMO system used in a mobile terminal [23]. The dimension of the system substrate is

The associate editor coordinating the review of this manuscript and approving it for publication was Zhen Gao.

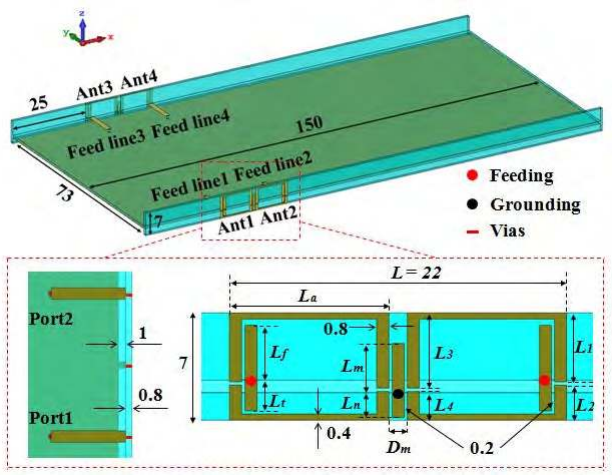

FIGURE 1. Geometry of the dual-band 4-antenna MIMO system composed of two compact self-decoupled antenna pairs. All units are in millimeters.

150mm×75mm×0.8mm, while the size of ground plane is 150mm×73mm (with a 1mm clearance along two side edges of the system substrate). Four antenna elements are printed separately on two antenna frames located at the left and right sides of the phone. The antenna frames, with a thickness of 0.8mm and a height of 7mm, are perpendicularly placed to the system substrate. The system substrate and the antenna frames are all based on FR4 (with $\varepsilon_r = 4.3$ and $\tan\delta = 0.02$). The total area occupied by two adjacent antennas, which refer as an antenna pair, is 22mm×7mm. Although the proposed compact antenna pair is located at the upper and lower sides (similar to the antenna configurations proposed in [3], [10]–[12], [16]) of the antenna frame, the dual-band operation is supported. The antenna pair consists of two identical antenna elements. Each antenna element has an I-shaped feeding strip, a large inverted U-shaped radiating branch (used to generate the 3.5GHz band) and a small U-shaped radiating branch (used to generate the 4.9GHz band). In particular, the two identical antenna elements share one common grounding branch, which is coupled with both the U-shaped radiating elements. The widths of the vertical trace and the horizontal trace of the antenna are fixed at 0.8mm and 0.4mm, respectively. The horizontal coupling gaps between the I-shaped feeding branch and the U-shaped branches, and the gaps between the grounding strip and the U-shaped elements are all fixed at 0.2mm. All the antennas are fed with 50 Ω SMA connectors through via-hole from the back side of the system substrate.

The detailed dimension of the antenna is set as follows. The length of the I-shaped feeding branch is described as $L_f + L_t$, where L_f and L_t are respectively the length above and below the horizontal plane of the feeding line. The upper feeding part L_f coupled with the large inverted U-shaped branch is used to generate the 3.5GHz band, whereas the lower feeding part L_t coupled with the small U-shaped branch is used to excite the 4.9GHz band. The lengths of four vertical strips of both the large and small U-shaped branches are described in sequence as L_1, L_2, L_3 and L_4. The lengths of the strips adjacent to the feeding element are separately described by L_1 and L_2, and the lengths of the strips close to the common grounding branch are described by L_3 and L_4, respectively. Similarly, the grounding branch contains two parts; and the lengths of the upper part (above the ground plane) and lower part (below the ground plane) are separately represented by L_m and L_n.

B. PARAMETER ANALASIS

Fig. 2 shows the simulated S-parameter of the proposed dual-band 4-antenna MIMO system with the optimized dimensions listed in Table 1. Because the 4-antenna system has certain symmetries, only necessary S-parameter will be given. As shown in Fig. 2, the MIMO antenna can well cover both the low band (i.e., 3.5GHz band) and the high band (i.e., 4.9GHz band) with the isolation, S12, better than −17.5dB for the low band and −20dB for the high band. It can also be seen from Fig. 2 that the isolations S13, S23 and S24 are always better than −24.8dB. The above results indicate that the proposed compact self-decoupled antenna pair can ensure good isolation between the two adjacent antennas.

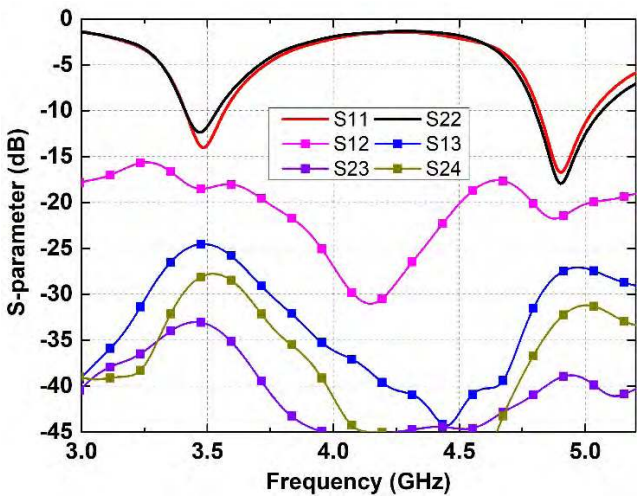

FIGURE 2. Simulated S-parameter of the proposed dual-band 4-antenna MIMO system.

TABLE 1. Optimized dimensions of the antenna.

Parameters	L_f	L_t	L_m	L_n	L_1	L_2
Value(mm)	3.6	2	3.2	1.6	4.5	2.3
Parameters	L_3	L_4	L_a	L	D_m	
Value(mm)	4.9	1.9	10.4	22	1.2	

The reflection coefficient of Ant1 and the isolation between Ant1 and Ant2 varied as functions of L_f and L_t are shown in Figs. 3 and 4, respectively. One can see from Fig. 3 that the value of L_f mainly affects the first resonance mode of the antenna unit; and the resonance frequency of this

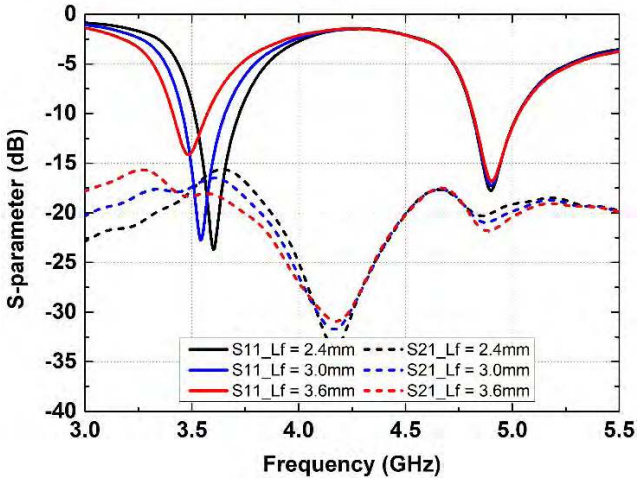

FIGURE 3. Simulated S-parameter of the proposed MIMO antenna system as a function of Lf.

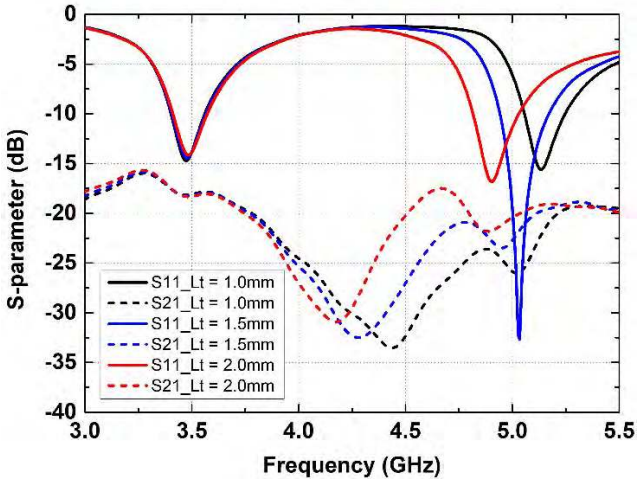

FIGURE 4. Simulated S-parameter of the proposed MIMO antenna system as a function of Lt.

mode shifts lower when L_f increases. In contrast, the second resonance mode of the antenna unit is affected by the value of L_t, as shown in Fig. 4, which indicates that the length of the lower part of the I-shaped feeding branch has quite significant impact on the resonance of the high band. It is worth mentioning that, when the length of the upper part (the lower part) of the feeding element varies, the performance of the high band (the low band) of the antenna almost does not change. This also means that changing the length of L_f (L_t) has very little impact on the isolation and return loss of the high band (low band). Therefore, the upper and lower parts of the antenna can be adjusted independently.

C. DECOUPLING ANALYSIS

To better understand the working principle of the proposed dual-band 4-antenna MIMO system, the simulated current distributions of Ant1 and Ant2 at 3.5GHz and 4.9GHz are given in Fig. 5. One can observe from Fig. 5 that when Ant1 is

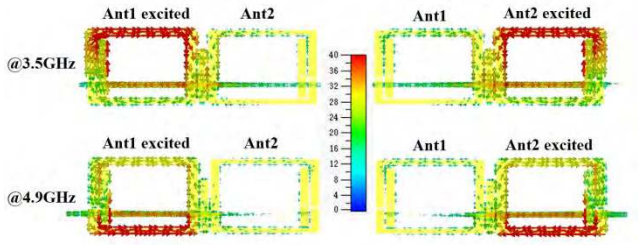

FIGURE 5. Simulated current distributions of Ant1 and Ant2 at 3.5GHz and 4.9GHz.

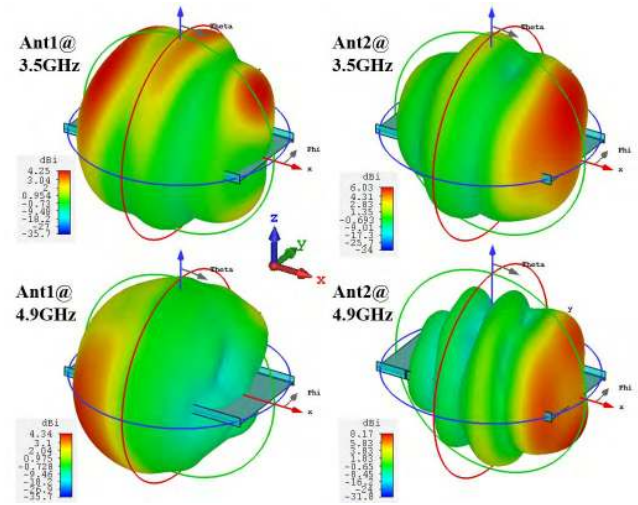

FIGURE 6. 3D radiation patterns of Ant1 and Ant2 of the proposed dual-band 4-antenna MIMO system at 3.5GHz and 4.9GHz.

excited, the current distribution of the low band (3.5GHz) is mainly concentrated on the large U-shaped branch of Ant1, whereas the current distribution of the high band (4.9GHz) is mainly concentrated on the small U-shaped branch of Ant1. Similar phenomenon can be observed for Ant2. This indicates that with the proposed dual-band self-decoupled antenna pair, the currents almost do not penetrate from one antenna element to another for both the low and high bands. This characteristic ensures good isolation between the two very close antennas. In addition, the simulated 3D radiation patterns of Ant1 and Ant2 of the proposed dual-band 4-antenna MIMO system at 3.5GHz and 4.9GHz are shown in Fig. 6. It can be seen from Fig. 6 that the radiation patterns between Ant1 and Ant2 are quite different. In addition, the maximum gains of Ant1 and Ant2 point to different directions, which also demonstrates that small envelope correlation coefficient (ECC) and good isolation can be obtained for both the low and high bands. Note that all the simulated results presented in this work are obtained with CST microwave studio [26].

To further demonstrate the working principle and merit of the proposed self-decoupled antenna pairs, the impact of the parameters L_m and L_n on the antenna performance is studied. The simulated S-parameter and the Smith chart of

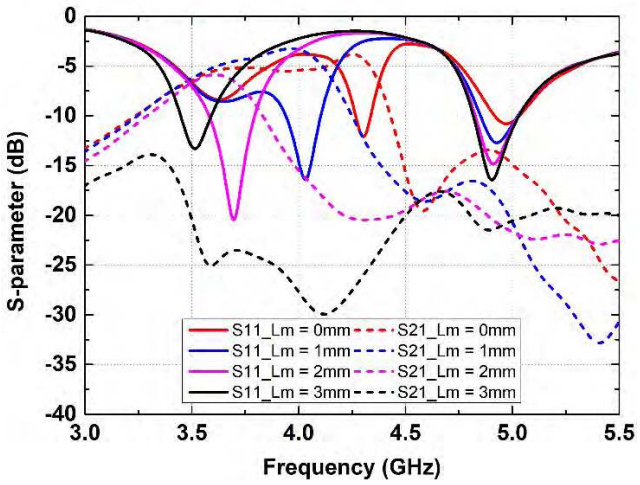

FIGURE 7. Simulated S-parameter of the MIMO antenna pair as a function of Lm while Ln is fixed at 1.6mm.

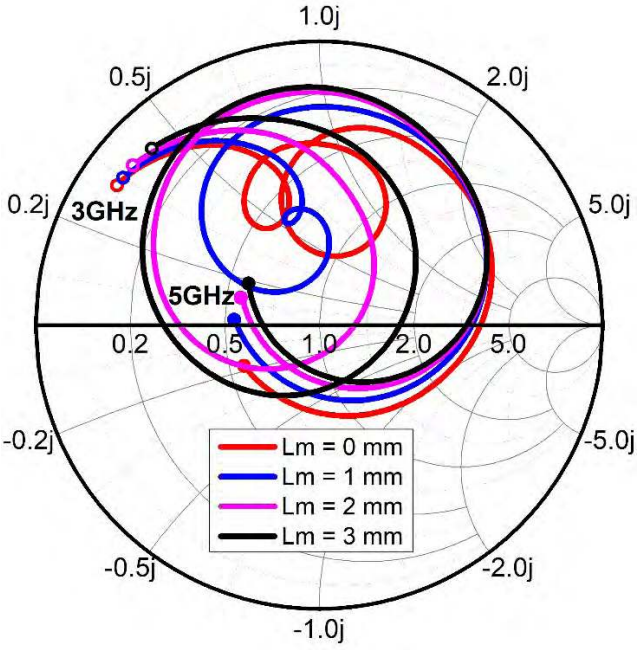

FIGURE 8. Simulated Smith Chart of the MIMO antenna pair as a function of Lm while Ln is fixed at 1.6mm.

the antenna pair as a function of L_m (while all the other optimized parameters listed in Table 1 are unchanged) are shown in Figs. 7 and 8, respectively. It can be seen from Figs. 7 and 8 that there are three resonance modes (at around 3.6GHz, 4.3GHz and 4.9GHz) within the frequency range of 3.0-5.0GHz when $L_m = 0.0$mm. In particular, the third resonance mode around 4.9GHz (i.e., the high band) is generated by the lower part of the antenna pair; and it is always true when L_m varies (from 0.0mm to 3.0mm). Because the third resonance mode is generated by the lower part of the antenna pair and its resonance frequency is almost unchanged when L_m varies from 0.0mm to 3.0mm, only the behavior of the first two resonance modes needs to be considered

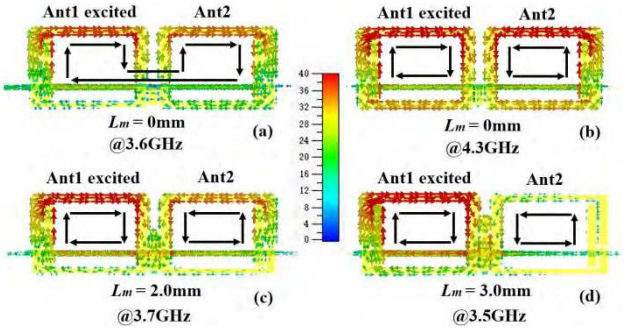

FIGURE 9. Comparison of the simulated current distributions for different cases: (a) 3.6GHz with Lm = 0.0mm; (b) 4.3GHz with Lm = 0.0mm; (c) 3.7GHz with Lm = 2.0mm; and (d)3.5GHz with Lm = 3.0mm.

when L_m varies. It can be seen from Figs. 7 and 8 that the first two resonance modes exist when $L_m = 0$mm or 1mm; and only a single resonance mode (around 3.5GHz) exists when $L_m = 3$mm. In particular, the antenna pair starts to change from the two resonance modes stage to the one single resonance mode stage when $L_m = 2.0$mm. In addition, when L_m varies from 0.0mm to 3.0mm, the existence of the first resonance mode that resonates at 3.6GHz (while existing) undergoes the following changes: from strong ($L_m = 0.0$mm) to medium ($L_m = 1.0$mm); from medium to weak ($L_m = 2.0$mm); and from weak to complete disappearance ($L_m = 3.0$mm). In contrast, however, the second resonance mode always exists when L_m varies from 0.0mm to 3.0mm; and its resonance frequency decreases from 4.3GHz ($L_m = 0.0$mm) to 4.0GHz ($L_m = 1.0$mm), 3.7GHz ($L_m = 2.0$mm), or 3.5GHz ($L_m = 3.0$mm). Therefore, increasing the height of the common grounding branch L_m actually can increase the effective length of the upper part of the antenna. One can also see from Fig. 7 that the isolation is quite bad when L_m varies from 0.0mm to 2.0mm; but it gets significantly improved when $L_m = 3.0$mm. This means that, when the value of L_m varies in the range of 0.0-3.0mm, the resonance mode of the low band that one expects to achieve from the self-decoupled antenna pair exists only when $L_m \geq 3.0$mm. Moreover, it can also be seen from Fig. 7 that the isolation of the high band is continuously improved when L_m increases from 0.0mm to 3.0mm. From the above one can obviously see the importance of the shared common ground branch. To further confirm the above phenomenon, the current distributions of the first resonance (3.6GHz) and second resonance (4.3GHz) when $L_m = 0.0$mm; the (second) resonance (3.7GHz) when $L_m = 2.0$mm; and the pure single resonance (3.5GHz) when $L_m = 3.0$mm are shown in Figs. 9(a), 9(b), 9(c), 9(d), respectively. One can see from Fig. 9(a) that when $L_m = 0.0$mm, the first resonance mode (3.6GHz) is generated by the upper part of the entire antenna pair (i.e., the combination of the upper parts of Ant1 and Ant2). In particular, at this frequency the current flows from the left (the upper part of Ant1) to the right (the upper part of Ant2) of the antenna pair; and the current loop of this mode is formed by the combination of the above currents and the current flowing on the ground plane. However, one

can see from Fig. 9(b) that there are two separate current loops for the second resonance mode (4.3GHz), which means that this second resonance mode is created by the upper part of Ant1 only. Obviously, this first resonance mode (3.6GHz) is not useful, which is because not only the isolation of this mode is too poor but also Ant1 or Ant2 does not work individually at all. In contrast, the second resonance mode (4.3GHz) has two separate current loops that are generated individually by the upper parts of Ant1 and Ant2. Nevertheless, this second resonance mode obtained with $L_m = 0$ mm is still not useful due to the poor isolation. By comparing the current distributions in Fig. 9(b) and Fig. 9(c), one can see that although less current is coupled from Ant1 to Ant2 when L_m increases from 0.0mm to 2.0mm, the coupling between Ant1 and Ant2 is still quite strong when $L_m = 2.0$mm, which still results in poor isolation and this mode is still not useful. In fact, this (second) mode will be useful only when the height of the common grounding branch L_m is bigger enough. For example, as shown in Fig. 9(d), insignificant current flows or couples from Ant1 to Ant2 when $L_m = 3.0$mm. Actually, the first resonance mode disappears completely when $L_m \geq 3.0$mm. Therefore, one can say that the antenna pair works as the proposed self-decoupled MIMO antenna pair only when $L_m \geq 3.0$mm.

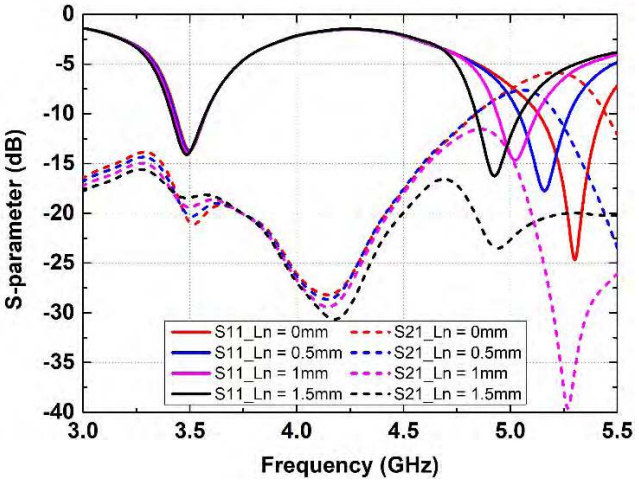

FIGURE 10. Simulated S-parameter of the MIMO antenna pair as a function of Ln while Lm is fixed at 3.2mm.

The simulated S-parameter of the antenna pair as a function of L_n (while all the other optimized parameters listed in Table 1 are unchanged) is shown in Fig. 10. One can see from Fig. 10 that the performance of the low band varies insignificantly when L_n varies. Hence, only the behavior of the high band needs to be considered when L_n varies. As the upper part and lower part of the antenna pair work almost independently, phenomena similar to the low band case (i.e., when L_m varies) can be observed for the high band when L_n varies. For example, the isolation for the high band is also improved significantly when L_n increases from 0.0mm to 1.5mm, as can be seen in Fig. 10. Similar to the behavior of the upper part of the antenna pair (i.e., the low band case), the lower part of the antenna pair works as the self-decoupled antenna pair for the high band when $L_n \geq 1.5$mm. From the above study, one can conclude that by adopting the common grounding for the proposed antenna pair, a compact dual-band self-decoupled MIMO antenna system can be realized.

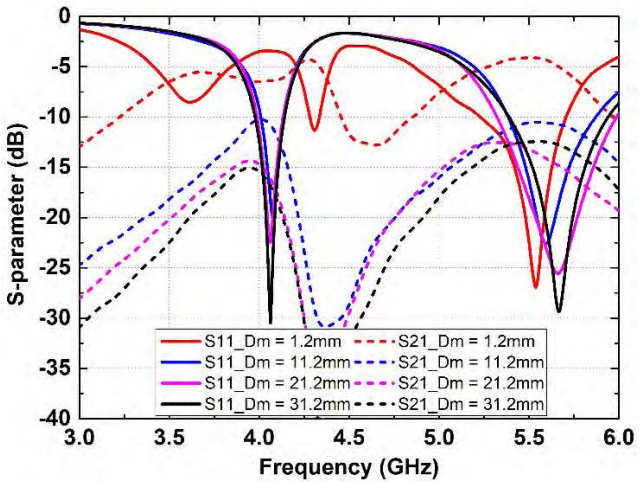

FIGURE 11. Simulated S-parameter of the MIMO antenna pair as a function of Dm, while Lm = 0.0 mm, Ln = 0.0mm and other parameters remain unchanged.

To even further demonstrate the usefulness of the common grounding branch, the S-parameter of the antenna pair without the common grounding branch (i.e., $L_m = L_n = 0.0$ mm) is studied. In particular, how the edge-to-edge distance, D_m, affects the S-parameter of the antenna pair is studied. When D_m increases, the location of Ant2 (and its counterpart Ant4) is moved along +x direction while the location of Ant1 (and its counterpart Ant3) is unchanged. One can see from Fig. 11, the isolation between Ant1 and Ant2 gets constantly improved when D_m increases from 1.2mm to 31.2mm. However, the isolation can only reach −15dB at the low band and −12.5dB at the high band even if the distance between two antennas reaches 31.2mm. Moreover, in this case the resonance frequency is around 4.05GHz at low frequency and 5.64GHz at high frequency, which is about 1.15 times (4.05GHz/3.5GHz for the low band and 5.64GHz/4.9GHz for the high band) bigger than the resonance frequencies of the proposed decoupled MIMO antenna pair. From the above analysis, one can conclude that the common grounding branch can not only improve the isolation of the MIMO antenna pair but also increase the effective length of the antenna element.

III. THE MEASURED RESULTS

A. ANTENNA PERFORMANCE

An antenna prototype of the proposed dual-band 4-antenna MIMO system with the optimized dimensions listed in Table 1 was fabricated and measured. The photo of the fabricated antenna prototype is shown in Fig. 12. The measured and simulated S-parameters are shown in Fig. 13. One can

FIGURE 12. Photo of the fabricated antenna prototype.

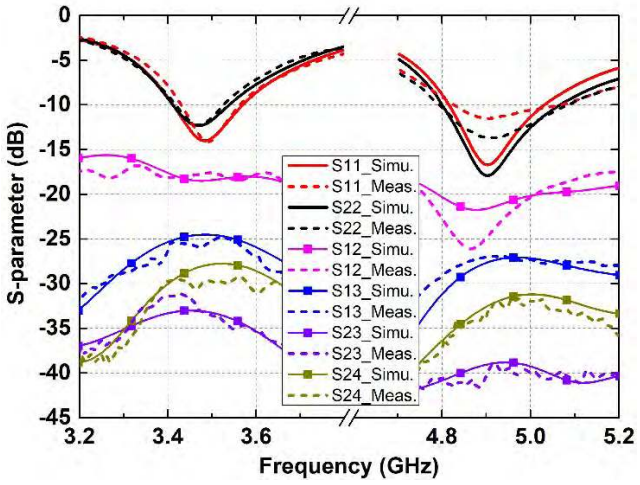

FIGURE 13. Simulated and measured S-parameters for the proposed 4-antenna MIMO system.

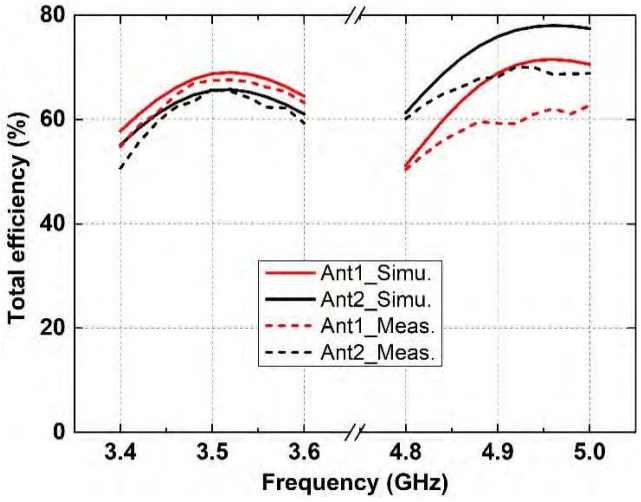

FIGURE 14. Simulated and measured total efficiencies for proposed 4-antenna MIMO system.

see from Fig. 13 that the both the simulated and measured isolations are well below −17dB in the low band and −20dB in the high band. The simulated and measured total efficiencies for the proposed dual-band 4-antenna MIMO system is shown in Fig. 14 and the measured total efficiency is over 50% for both the low and high bands. Also, good agreement between the measured and simulated results can be observed.

The simulated and measured 2D radiation patterns of Ant1 and Ant2 in the xoy, xoz and yoz planes at two

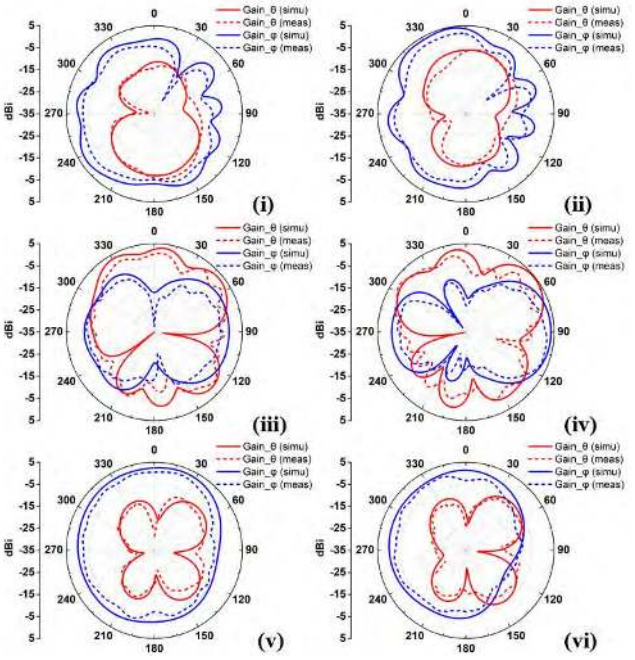

FIGURE 15. 2D antenna radiation patterns of Ant1 and Ant2 of 4-antenna MIMO system at 3.5GHz. (i) Ant1 in xoy plane. (ii) Ant2 in xoy plane. (iii) Ant1 in xoz plane. (iv) Ant2 in xoz plane. (v) Ant1 in yoz plane. and (vi) Ant2 in yoz plane.

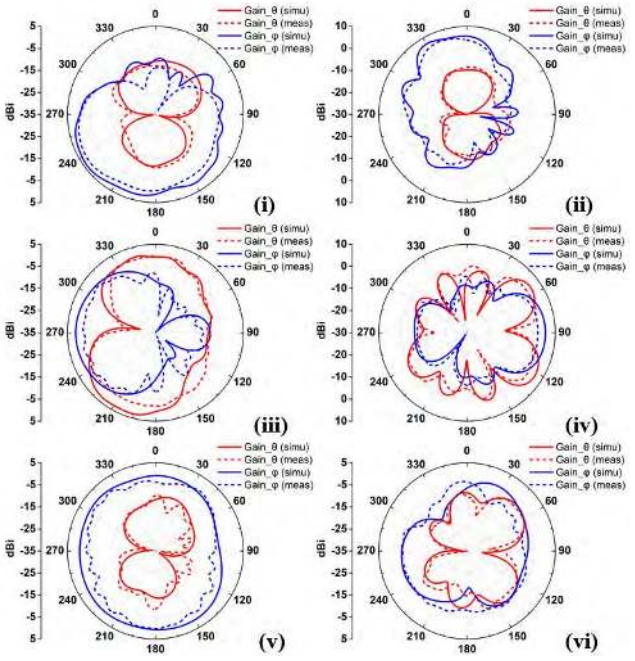

FIGURE 16. 2D antenna radiation patterns of Ant1 and Ant2 of 4-antenna MIMO system at 4.9GHz. (i) Ant1 in xoy plane. (ii) Ant2 in xoy plane. (iii) Ant1 in xoz plane. (iv) Ant2 in xoz plane. (v) Ant1 in yoz plane. and (vi) Ant2 in yoz plane.

different frequencies 3.5GHz and 4.9GHz are shown in Figs. 15 and 16, respectively; and good agreement is obtained between the simulation and measurement. One can see from Figs. 15 and 16 that each antenna has a unique radiation pattern. This behavior can ensure smaller ECC for the antenna

pair, and thereby an enhanced channel capacity (CC) for the MIMO operation can be obtained.

B. MIMO PERFORMANCES

To quantitatively evaluate the performance of the proposed dual-band MIMO antenna system, the envelope correlation coefficient and the channel capacity of a 4×4 MIMO system are analyzed. For simplification, it is assumed that multipath environment is isotropic in the sense of both power density and polarizations [27]. Therefore, the envelope correlation between antenna i and antenna j can be calculated by the complex radiation far field as follows:

$$ECC(i,j) = \frac{\left|\oint\oint A_{ij}(\theta,\varphi)sin\theta d\theta d\varphi\right|^2}{\oint\oint A_{ii}(\theta,\varphi)sin\theta d\theta d\varphi \cdot \oint\oint A_{jj}(\theta,\varphi)sin\theta d\theta d\varphi} \quad (1)$$

where

$$A_{ij}(\theta,\varphi) = E_{\theta,i}(\theta,\varphi)\cdot E^*_{\theta,j}(\theta,\varphi) + E_{\varphi,i}(\theta,\varphi)\cdot E^*_{\varphi,j}(\theta,\varphi) \quad (2)$$

and the simulated and measured complex radiation far field of the antennas can be obtained from either CST or 3D measurement in an anechoic chamber.

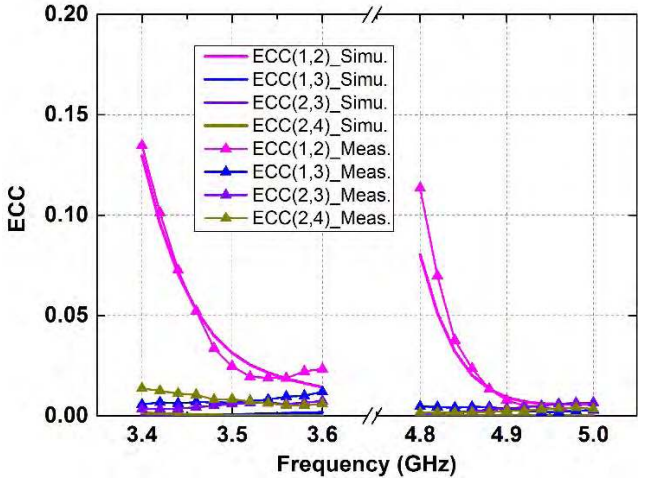

FIGURE 17. Calculated envelope correlation coefficient (ECC) values from the simulated and measured results.

The simulated and measured ECCs of the proposed MIMO antenna system are illustrated in Fig. 17. It should be noted here that the simulated ECC means that the value of ECC is calculated from the complex radiation far field of the antennas obtained directly from CST; whereas the measured ECC means that the value of ECC is calculated from the measured complex radiation far field of the antennas. One can see that the value of the simulated and measured ECCs are smaller than 0.14 in the low band and 0.12 in the high band, which are all good enough for the 5G MIMO operation.

The channel capacity (CC) that is used to evaluate the performance of MIMO systems can be defined as follows:

$$CC = E\left\{\log_2\left[det\left(I + \frac{SNR}{n_T}\right)H_{scale}H^T_{scale}\right]\right\} \quad (3)$$

and the channel matrix Hscale can be calculated as follow:

$$H_{scale} = \sqrt{\rho_{scale,RX}}H_{\text{i.i.d}}\sqrt{\rho_{scale,TX}} \quad (4)$$

and as explained in [28], the antenna total efficiency needs to be taken into account when the channel capacity of the MIMO antenna system is calculated:

$$\rho_{scale,RX} = \sqrt{\eta_{total}}\rho_{RX}\sqrt{\eta_{total}} \quad (5)$$

The E in Eq. (3) denotes the expectation with respect to different channel realizations, I is an identity matrix, SNR is the mean signal-to-noise ratio at the receiving side, nT is the number of transmitting antennas, and $(.)^T$ denotes the Hermitian transpose. In this study, it is assumed that the transmitting antennas are uncorrelated (i.e., ECC = 0 at transmitting side) whereas the four antenna elements of the proposed antenna array serve as the receiving antennas with the envelope correlation coefficient ρ_{RX} (i.e., ECC) and total efficiency η_{total}. And the $H_{i.i.d}$ is a 4 × 4 matrix, in which the entries are independent identically distributed complex Gaussian variables. The measured CC of the 4 × 4 MIMO antenna system obtained by averaging over 10,000 Rayleigh fading realizations with SNR = 20dB [3], [14], [15] are shown in Fig. 18. The measured CC means that the value of CC is calculated from the measured antenna total efficiency and the measured ECC. The calculated channel capacity within the operating bands is in the range of 15.3-18.3bps/Hz, whereas the ideal 4 × 4 MIMO system is about 22bps/Hz.

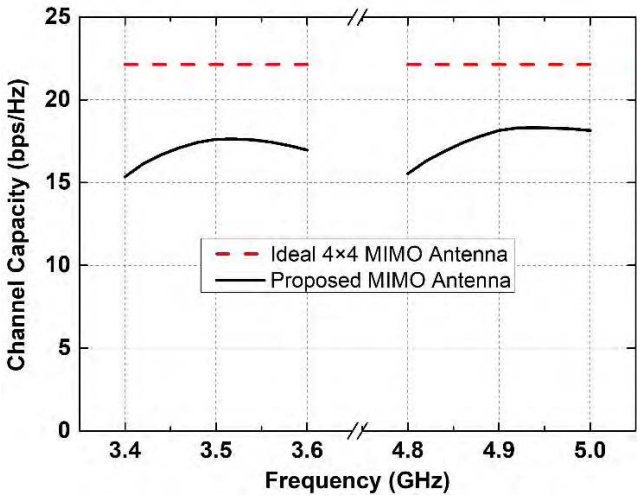

FIGURE 18. Calculated ergodic channel capacity (CC) values from the measured results.

IV. PRACTICAL APPLICATION DISCUSSION

A. DISPLAY PANEL EFFECTS

To study the influence of the display panel, a glass ($\varepsilon_r = 5.5$) with the size of 140mm×75mm×2mm is added above the ground plane and the spacing between the display panel and antenna traces is 0.8 mm. The reflection coefficients and isolations for the with display panel case and the without display panel case are illustrated in Fig. 19. The reflection

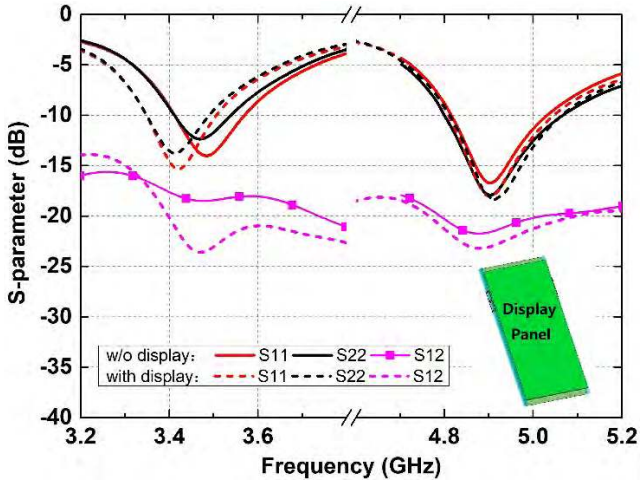

FIGURE 19. Simulated S-parameter of the 4 × 4 MIMO system with and without display panel.

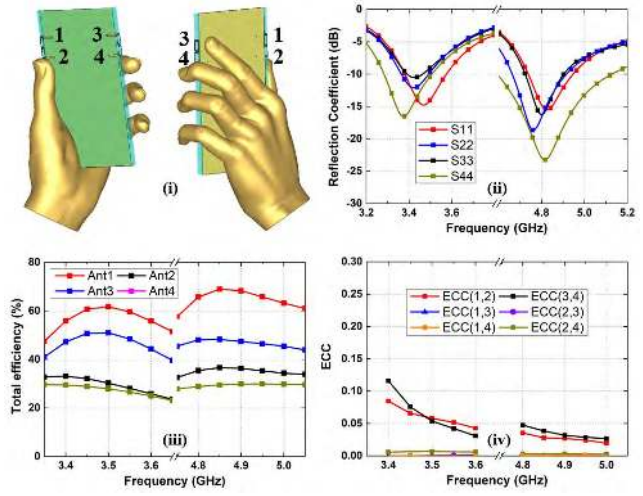

FIGURE 20. Simulated results with user's hand of the proposed 4 × 4 MIMO system. (i) Single-handhold scenario. (ii) Reflection coefficient. (iii) Antenna efficiency. (iv) Envelope correlation coefficient.

coefficients S11 and S22 have small frequency shifts to lower frequency in the low band, while they are almost unchanged in the high band. This is because the display panel is on the front side of the ground plane that is close to the upper branches of the antenna pairs. The isolation that is better than −20 dB can still be obtained even when the display panel is adopted. This means that the characteristic of the self-decoupled antenna pair is kept unchanged while the display panel is adopted. As a consequence, the proposed MIMO system is feasible in the practical environment or application.

B. USERS'S HAND EFFECTS

Finally, the hand effect on the performance of the proposed 4-antenna MIMO system will be studied. The simulated reflection coefficient, the antenna total efficiency as well as the envelope correlation coefficient of the proposed 4-antenna MIMO system with a phantom hand are shown in Fig. 20. It can be seen from Fig. 20 that the reflection coefficients for all the antennas are well below −6dB. The S-parameter results certainly indicate that the proposed dual-band 4-antenna MIMO system works well when it is held by the phantom hand. Compared to the free space case, the antenna total efficiencies drop for the with hand case. In particular, the antenna with the most phantom hand coverage suffers bigger efficiency degradation, as expected. However, the worst antenna efficiency is still better than 23%, which is still acceptable. Meanwhile, all the ECC values are less than 0.12 in the desired operating bands with the phantom hand, which is also acceptable for practical scenario.

V. CONCLUSION

In this paper, a dual-band 4-antenna MIMO system based on the compact self-decoupled antenna pairs for 5G applications in mobile terminals is proposed. In particular, the antenna pair contains two parts: the upper part and the lower part. The low band is generated by the upper part, whereas the high band is created by the lower part. By adopting the common grounding branch as the decoupling element between the two adjacent antennas, quite good isolation can be obtained for both the low and high bands even when the two antennas are located very close to each other. Since the proposed solution can have compact antenna structure as well as high isolation and good antenna efficiency, it is very promising for practical 5G multiband MIMO applications in mobile terminals.

REFERENCES

[1] J. G. Andrews, S. Buzzi, W. Choi, S. V. Hanly, A. Lozano, A. C. K. Soong, and J. C. Zhang, "What will 5G be?" *IEEE J. Sel. Areas Commun.*, vol. 32, no. 6, pp. 1065–1082, Jun. 2014.

[2] Y. S. Cho, J. Kim, W.-Y. Yang, and C. G. Kang, *MIMO-OFDM Wireless Communications with MATLAB*. New York, NY, USA: Wiley, 2010.

[3] A. A. Ai-Hadi, J. Ilvonen, R. Valkonen, and V. Viikari, "Eight-element antenna array for diversity and MIMO mobile terminal in LTE 3500 band," *Microw. Opt. Technol. Lett.*, vol. 56, pp. 1323–1327, Jun. 2014.

[4] K.-L. Wong, J.-Y. Lu, L.-Y. Chen, W.-Y. Li, and Y.-L. Ban, "8-antenna and 16-antenna arrays using the quad-antenna linear array as a building block for the 3.5-GHz LTE MIMO operation in the smartphone," *Microw. Opt. Technol. Lett.*, vol. 58, pp. 174–181, Jan. 2016.

[5] J. L. Guo, L. Cui, C. Li, and B. H. Sun, "Side-edge frame printed eight-port dual-band antenna array for 5G smartphone applications," *IEEE Trans. Antennas Propag.*, vol. 66, no. 12, pp. 7412–7417, Dec. 2018.

[6] Y. Li, C.-Y.-D. Sim, Y. Luo, and G. Yang, "Metal-frame-integrated eight-element multiple-input multiple-output antenna array in the long term evolution bands 41/42/43 for fifth generation smartphones," *Int. J. RF Microw. Comput.-Aided Eng.*, vol. 29, no. 1, Jan. 2019, Art. no. e21495.

[7] M.-Y. Li, Y. L. Ban, Z. Q Xu, G. Wu, C. Sim, K. Kang, and Z. F. Yu, "Eight-port orthogonally dual-polarized antenna array for 5G smartphone applications," *IEEE Trans. Antennas Propag.*, vol. 64, no. 9, pp. 3820–3830, Sep. 2016.

[8] M.-Y. Li, Z.-Q. Xu, Y.-L. Ban, C.-Y.-D. Sim, and Z.-F. Yu, "Eight-port orthogonally dual-polarised MIMO antennas using loop structures for 5G smartphone," *IET Microw., Antennas Propag.*, vol. 11, pp. 1810–1816, Dec. 2017.

[9] M. Y. Li, Y. L. Ban, Z. Q. Xu, J. Guo, and Z. F. Yu, "Tri-polarized 12-antenna MIMO array for future 5G smartphone applications," *IEEE Access*, vol. 6, pp. 6160–6170, Jan. 2018.

[10] K.-L. Wong, C.-Y. Tsai, and J.-Y. Lu, "Two asymmetrically mirrored gap-coupled loop antennas as a compact building block for eight-antenna MIMO array in the future smartphone," *IEEE Trans. Antennas Propag.*, vol. 65, no. 4, pp. 1765–1778, Apr. 2017.

[11] K. L. Wong, B. W. Lin, and W. Y. Li, "Dual-band dual inverted-F/loop antennas as a compact decoupled building block for forming eight 3.5/5.8-GHz MIMO antennas in the future smartphone," *Microw. Opt. Technol. Lett.*, vol. 59, pp. 2715–2721, Nov. 2017.
[12] C. Y. Tsai, K. L. Wong, and W. Y. Li, "Experimental results of the multi-Gbps smartphone with 20 multi-input multi-output (MIMO) antennas in the 20×12 MIMO operation," *Microw. Opt. Technol. Lett.*, vol. 60, pp. 2001–2010, Aug. 2018.
[13] H. Xu, H. Zhou, S. Gao, H. Wang, and Y. Cheng, "Multimode decoupling technique with independent tuning characteristic for mobile terminals," *IEEE Trans. Antennas Propag.*, vol. 65, no. 12, pp. 6739–6751, Dec. 2017.
[14] A. Zhao and Z. Ren, "Multiple-input and multiple-output antenna system with self-isolated antenna element for fifth-generation mobile terminals," *Microw. Opt. Technol. Lett.*, vol. 61, pp. 20–27, Jan. 2019.
[15] A. Zhao and Z. Ren, "Size reduction of self-isolated MIMO antenna system for 5G mobile phone applications," *IEEE Antennas Wireless Propag. Lett.*, vol. 18, no. 1, pp. 152–156, Jan. 2019.
[16] L. B. Sun, H. Feng, Y. Li, and Z. Zhang, "Compact 5G MIMO mobile phone antennas with tightly arranged orthogonal-mode pairs," *IEEE Trans. Antennas Propag.*, vol. 66, no. 11, pp. 6364–6369, Nov. 2018.
[17] Y.-L. Ban, C. Li, C.-Y.-D. Sim, G. Wu, and K.-L. Wong, "4G/5G multiple antennas for future multi-mode smartphone applications," *IEEE Access*, vol. 4, pp. 2981–2988, 2016.
[18] Z. Ren, S. Wu, and A. Zhao, "Coexist design of sub-6GHz and millimeter-wave antennas for 5G mobile terminals," in *Proc. Int. Symp. Antennas Propag. (ISAP)*, Busan, South Korea, Oct. 2018, pp. 805–806.
[19] K.-L. Wong and J. Y. Lu, "3.6-GHz 10-antenna array for MIMO operation in the smartphone," *Microw. Opt. Technol. Lett.*, vol. 57, no. 7, pp. 1699–1704, Jul. 2015.
[20] J. Y. Deng, J. Yao, D. Q. Sun, and L. X. Guo, "Ten-element MIMO antenna for 5G terminals," *Microw. Opt. Technol. Lett.*, vol. 60, pp. 3045–3049, Dec. 2018.
[21] Y. Li, C.-Y.-D. Sim, Y. Luo, and G. Yang, "12-port 5G massive MIMO antenna array in sub-6GHz mobile handset for LTE bands 42/43/46 applications," *IEEE Access*, vol. 6, pp. 344–354, Feb. 2018.
[22] Y. Li, C.-Y.-D. Sim, Y. Luo, and G. Yang, "Multiband 10-antenna array for sub-6 GHz MIMO applications in 5-G smartphones," *IEEE Access*, vol. 6, pp. 28041–28253, Jun. 2018.
[23] Z. Ren and A. Zhao, "Compact dual-band 5G MIMO antenna system and mobile terminal," China Patent 2019 207 173 461, May 20, 2019.
[24] *5G NR (New Radio)*. Accessed: Nov. 15, 2018. [Online]. Available: http://3gpp.org/
[25] Asia Times. *China Reserves Spectrum for 5G Services*. Accessed: Nov. 16, 2017. [Online]. Available: http://www.atimes.com/article/china-reserves-spectrum-5g-services/
[26] *CST 2018*. Accessed: Nov. 15, 2018. [Online]. Available: https://www.cst.com/
[27] Z. Zhang, *Antenna Design for Mobile Devices*, 2nd ed. Hoboken, NJ, USA: Wiley, 2017.
[28] J. X. Yun and R. G. Vaughan, "Multiple element antenna efficiency and its impact on diversity and capacity," *IEEE Trans. Antennas Propag.*, vol. 60, no. 2, pp. 529–539, Feb. 2012.

ZHOUYOU REN (M'19) received the B.Sc. degree in communication engineering from Beijing Jiaotong University, Beijing, China, in 2014, and the M.Sc. degree in data communication from The University of Sheffield, U.K., in 2016.

In 2017, he joined Shenzhen Sunway Communication Company Ltd., as an RF Engineer, and became a Senior RF Engineer, in 2019. His current research interests include antenna decoupling techniques and millimeter-wave antennas, and MIMO antenna system for 5G applications.

ANPING ZHAO (M'90–SM'98) received the B.Sc. degree in optical physics from the Changchun University of Science and Technology, China, in 1984, the M.Sc. degree in optics from the Changchun Institute of Physics, Chinese Academy of Sciences, China, in 1987, and the Ph.D. degree in electronic and electrical engineering from Brunel University, London, U.K., in 1994.

From 1987 to 1989, he was a Researcher with the Changchun Institute of Physics. In 1990, he joined the Department of Electronic and Electrical Engineering, Surrey University, Surrey, U.K., as a Visiting Research Fellow, where he was involved on the computer verification of optical waveguide characteristics based on multiple-quantum-well (MWQ) structures in III–V semiconductor materials. In 1994, he joined the Radio Laboratory, Department of Electrical and Communications Engineering, Helsinki University of Technology, Helsinki, Finland, where he was involved on the computer-aided-design of microwave and millimeter-wave circuits with the FDTD method. He joined the Nokia Research Center, in 1997. From 1997 to 2007, he was a Senior Research Engineer/Principal Researcher, with the Nokia Research Centre, Helsinki. From 2007 to 2012, he was a Principal Scientist with the Nokia Research Center, Beijing, China. In 2012, he joined Shenzhen Sunway Communication Company Ltd., as the Chief Technical Expert and the Director of the Advanced Antenna Technology Department. His current research interests include antenna designs for 4G LTE, MIMO antenna system and millimeter-wave antenna designs for 5G applications, and other antennas used in portable devices. He has authored more than 120 refereed papers. He holds about 30 granted invention patents. He is listed in Marquis Who's Who in the World and Who's Who in Sciences and Engineering.